Composites Part B 293 (2025) 112143

Contents lists available at ScienceDirect

Composites Part B

journal homepage: www.elsevier.com/locate/compositesb

CFRP laminate with autonomous sensing and enhanced impact resistance by P(VDF-TrFE) nanofibers interleaving

Francesco Mongioì [a], Giacomo Selleri [a,*], Emanuele Maccaferri [b], Davide Fabiani [c], Andrea Zucchelli [a], Tommaso Maria Brugo [a,**]

[a] Department of Industrial Engineering, University of Bologna, Viale Risorgimento 2, 40136, Bologna, Italy
[b] Department of Industrial Chemistry "Toso Montanari", University of Bologna, Viale Risorgimento 4, 40136, Bologna, Italy
[c] Department of Electrical, Electronic, and Information Engineering, University of Bologna, Viale Risorgimento 2, 40136, Bologna, Italy

ARTICLE INFO

Handling Editor: Prof. Ole Thomsen

Keywords:
Piezoelectric
PVDF nanofibers
Smart materials
Structural health monitoring
Electrical properties

ABSTRACT

Structural Health Monitoring (SHM) techniques have been developed to watch over the health status of composite structures and increase their safety. However, these techniques are traditionally based on the embedding of sensors that could compromise the inherent strength of the hosting laminate. In this work, a novel approach to confer a sensing capability to Carbon Fiber Reinforced Plastic (CFRP) laminates is proposed by interleaving piezoelectric poly(vinylidene fluoride–trifluoroethylene) (P(VDF-TrFE)) nanofibers, and exploiting carbon fibers as electrodes to collect the piezoelectric signal. LVI test revealed an impact sensitivity equal to 233 mV/kN and an improved impact resistance compared to the non-sensing reference laminate, thanks to the interleaved nanofibers that hinder delamination. The impact resistance enhancement marks a paradigm shift with respect to the traditional integration of commercial sensors. Moreover, post-impact electrical measurements demonstrated the capability of detecting damage developed internally in the laminate. This innovative design introduces a new class of autonomous, self-sensing composite for aerospace applications to confer SHM capabilities without affecting or even incrementing the mechanical properties of the hosting laminate.

1. Introduction

Aerospace engineering is undergoing a transformation, shifting towards the utilization of carbon fiber composites over traditional metal alloys in aircraft construction. This transition is driven by the need to enhance performance and reduce weight amidst escalating fuel costs and stringent environmental regulations affecting commercial aviation. Composite materials, extensively employed in both primary and secondary structural components, play a pivotal role in advancing the high-tech aerospace industry. Notably, the 787 Dreamliner (a long-range airliner) exemplifies this shift, featuring 80 % composite by volume (approximately 32,000 kg of CFRP composites) [1–3].

Despite the evident benefits of composite materials in terms of performance and weight reduction, they present significant challenges, particularly concerning damage resistance. The mechanisms behind the damage and failure of metallic structures are generally well comprehended, primarily attributed to fatigue cracks that develop under cyclic loading in metal materials during service. Conversely, damage in composite materials manifests through a broader range of mechanisms compared to metals [4], including hidden damage from low-velocity impacts. This barely visible damage, or BVD, often manifests as delamination within the composite layup, which can bring sudden catastrophic failure, compromising compression strength and structural integrity [5,6].

Detecting and addressing in-service damage in composites pose unique challenges. While various Non-Destructive Evaluation (NDE) methods such as visual inspection, ultrasonics, radiography, and thermography are employed during routine maintenance, these inspections necessitate aircraft downtime, suspending normal operations. Consequently, there remains a possibility of undetected damage progression between scheduled inspections. Structural Health Monitoring (SHM) aims to improve the safety of structures and reduce control downtime by integrating onboard inspection technologies adapted from NDE, it must also evaluate the remaining useful life of the structure [6].

Typically, SHM systems incorporate sensors that may either be affixed to the surface of the laminate [7,8] or integrated within its layers

* Corresponding author.
** Corresponding author.
E-mail addresses: giacomo.selleri2@unibo.it (G. Selleri), tommasomaria.brugo@unibo.it (T.M. Brugo).

https://doi.org/10.1016/j.compositesb.2025.112143
Received 14 June 2024; Received in revised form 8 November 2024; Accepted 8 January 2025
Available online 10 January 2025

[9]. Nevertheless, environmental conditions may adversely impact the sensors' functionality when externally placed and embedding them could detrimentally influence the mechanical properties of the laminate [10]. PZT is commonly used for impact localization through elastic wave detection, thanks to their high sensitivity [11], while FBG is usually used for in plain strain measurement [12–14], and recently for impact localization [15–17]. However, due to their discrete distribution, the impact force estimation can be indirectly measured with less precision than a self-sensing laminate, where the sensing element is distributed on its whole surface.

The embedding of a brittle ceramic Lead Zirconate Titanate (PZT) piezoelectric sensor represents a defect that could initiate the crack propagation [18], and the interleaving of FBG generates a resin pocket, when transversally placed to the fibers, which causes stress and strain concentration in and around the optical fiber [19–21]. Subsequently, the focus has shifted towards the use of low-invasive techniques, by incorporating sub-micrometric materials between the laminate's plies to minimize the elastic properties mismatches. Ceramic and polymeric piezoelectric materials are particularly suitable for this purpose, as different manufacturing techniques can be used to tailor the desired size and shape (i.e., electrospinning, 3D printing, spin coating). With respect to traditional PZT sensors, the fabrication of PZT in the shapes of micro powder [18] or microfibers [22] improved the impact strength and the shear strength of the laminate. Similarly, other works reported on the possibility of substituting piezoelectric commercial sensors with nanoparticles dispersed in the epoxy matrix [23,24]. Beyond ceramic materials, piezoelectric polymers have been widely exploited for the functionalization of composite laminates, due to their easy-processability and intrinsic toughness. Among them, polyvinylidene fluoride (P(VDF)) in the shape of film has been embedded in Glass Fiber Reinforced Plastics (GFRP) to monitor three-point bending loadings [25], the damage and fatigue evolution [26]. Bae et al. interleaved a poly(vinylidene fluoride–trifluoroethylene) (P(VDF-TrFE)) film sensor between the CFRP plies to monitor low-velocity impact-induced damages, such as cracks or delamination. Investigations on the effect of the P(VDF-TrFE) film interleaving showed a degradation rate equal to 7–8% on Young's modulus, strength, and inter-laminar shear strength [27]. A consolidated strategy to reduce the intrusiveness of P(VDF) on the hosting structure is to fabricate it in the shape of nanofibers, produced via electrospinning. As demonstrated in Refs. [28–30], the integration of a negligible amount of polymeric nanofibers within the plies of a composite laminate resulted in an increase in the composite toughness. This effect is mainly attributable to the random disposition of the nanofibers interleaved in the composite laminates, which locally enhance the toughness of the interlayer [31–33].

Moreover, the composite laminate functionalization involves the insertion of electrodes in the stacking sequence to collect the piezoelectric signal. Traditional metallic electrodes such as aluminum foils or brass sheets could plasticize during impacts, likely leading to debonding and delamination, as previously investigated for Fiber Metal Laminates (FMLs) [18,29,34–37]. An alternative strategy could exploit the electrical properties of the carbon fibers, whose conductivity has been studied both as dry tows [38] and integrated into the epoxy matrix [39,40]. Recent advances pointed out the possibility of exploiting the electrical conductivity of carbon fibers to realize in-situ electrodes [41,42], without additional materials which could negatively impact the mechanical properties of CFRP. However, the main drawback related to this technique regards the connection of the acquisition circuit with the carbon fibers. For instance, Wang et al. used copper tape [43], and hybrid prepregs CFRP co-woven with copper wires were designed [44] to collect the piezoelectric signals, while Totoroki et al. painted a silver paste on CFRP laminate to monitor delamination with an electric resistance change method [45].

This work aims to confer self-sensing capabilities to a CFRP laminate by minimizing the impact on its mechanical properties, in contrast to the effects typically observed with the integration of commercial sensors. The novel approach consists of interleaving piezoelectric P(VDF-TrFE) nanofibers at the laminate's midplane and using the adjacent CFRP plies as electrodes, both for signal collection and electric poling. To erase triboelectric noise, CFRP-based shield electrodes are externally stacked in a sandwich-like structure, and electrically insulated by the signal electrodes by interleaving Nylon 6,6 nanofibers.

The experimental campaign is specifically designed to assess the self-sensing capability and the enhancement of the fracture toughness performance of the nano-modified laminate in comparison to the corresponding non-functionalized CFRP laminate. Additionally, the capability to detect inter-ply damage was investigated by a simple measurement of electrical resistance and capacitance between layers that does not require downtime as in traditional NDE methods.

In the SHM field, the proposed self-sensing laminate introduces a novel class of composite materials that can detect external mechanical loads and self-monitor its internal damage state, while enhancing its mechanical performances.

2. Materials & methods

2.1. Fabrication process of the autonomous self-sensing laminate

2.1.1. Electrospinning of the piezoelectric and insulating nanofibrous interlayer

Two different electrospinning processes have been used to fabricate P(VDF-TrFE) and Nylon-6,6 nanofibers. The former polymer is responsible for the sensing performances of the laminate. On the other hand, the Nylon-6,6 nanofibers are used as an insulating layer to prevent short-circuiting between two consecutive electrodes (i.e., CFRP plies used for the signal and shield electrodes).

The piezoelectric nanofibrous non-woven mat was electrospun starting from a polymeric solution prepared by dissolving 20 wt% of the copolymer P(VDF-TrFE) (70/30 mol%, M_w = 200 kDa, kindly provided by Solvay S.p.A. Milan, Italy, https://www.solvay.-com, Curie temperature T_c = 103 °C and melting temperature T_m = 145 °C) in dimethylformamide (DMF) (45 wt%) and acetone (55 wt%).

The polymeric solution for the fabrication of the insulating non-woven mat of Nylon-6,6 nanofibers was made by dissolving 10 wt% of Nylon-6,6 (Zytel E53NC010, DuPont) in a mixture of formic acid and chloroform (50:50 v/v).

For both the polymers, the electrospinning process was carried out in a four needle - drum collector electrospinning machine (Lab Unit, Spinbow®).

The P(VDF-TrFE) nanomat was electrospun by applying 19 kV to the high-voltage needles and collecting the randomly oriented nanofibers on the grounded rotating drum (0.4 m/s tangential speed), which was placed 18 cm away from the needles. The electrospinning processes were carried out with a flow rate equal to 0.75 ml/h per nozzle, at 24 °C and 40 % of relativity humidity (RH) until a grammage of 32 g/m^2 was obtained.

The Nylon-6,6 nanomat was electrospun by applying 27 kV to the high-voltage needles and collecting the randomly oriented nanofibers on the grounded rotating drum (0.4 m/s tangential speed), which was placed 15 cm away from the needles. The electrospinning processes were carried out with a flow rate equal to 0.50 ml/h per nozzle, at 24 °C and 40 % of relativity humidity (RH) until a grammage of 8 g/m^2 was obtained.

To fabricate an A3 size of the aforementioned nanomats, it took around 15 h. However, the parameter can be tuned to tailor the nanomat size and morphology [46,47], and the production rate can be scaled up to 20000 m^2/year with an industrial needleless electrospinning machine such as Elmarco (www.elmarco.com), to drastically reduce both production time and fabrication costs.

2.1.2. Carbon fibers electrical functionalization

Prior to stacking and fabricating the autonomous self-sensing

composite laminate, investigations have been performed to evaluate the properties of CFRP electrodes in terms of electrical conductivity, connection resistance, and mechanical integration of the signal cables with the CFRP plies. In particular, a thin copper wire (coil windings for high-frequency transformers, Ø = 80 μm) was used to electrically connect the unidirectional (UD) carbon fiber (T700S 250 g/m^2) epoxy matrix (T_g = 120 °C) prepreg (by Reglass) with the acquisition circuit. Three different stacking sequences were proposed by varying the mutual orientation between the carbon fibers of two UD CFRP plies. The configurations are [0°,0°], [0°,90°] and [90°,90°]. Two copper wires were interleaved at the opposite edges of the specimen, as shown in Fig. 1. Before stacking, the insulating jacket (polyurethane resin) of the copper wires portion to be interleaved was removed by soaking them in a DMF bath for 1 h. For each configuration, three specimens of 1 cm width (W) and variable length (L = 10, 20, and 30 cm) were stacked and cured in an autoclave at 6 bar and 100 °C for 4 h. The electrical resistance was measured for each sample by connecting the copper wires to an RLC meter (GW-Instek 6002).

2.1.3. Staking sequence and curing

The stacking sequence of the autonomous self-sensing composite laminate is [(CFRP-90°)/(CFRP-0°)/Ny_{nf}/(CFRP-90°)/(CFRP-0°)/P(VDF-TrFE)$_{nf}$]$_s$ as schematically represented in Fig. 2. The external pairs of CFRP plies (50 × 50 mm) serve as shield electrodes to erase triboelectric noise, which could affect the piezoelectric signal. The adjacent Nylon-6,6 nanofiber membranes are stacked to electrically insulate the shield electrodes and the signal electrodes (35 × 35 mm). At the midplane, the piezoelectric nanofibrous mat acts both as a charge generator and an insulating layer between the two adjacent signal electrodes. In addition to the functionalization of composite materials, the experimental campaign of this work also aims to evaluate the mechanical properties of the self-sensing laminates compared to those without nanofibers, named reference laminates. As observable from the photos of Fig. 2, the dimension and the stacking sequence of the CFRP plies are the same as the self-sensing laminates, but no nanofibers were interleaved [90°/0°/90°/0°]$_s$.

Nine replications were fabricated both for the self-sensing and reference laminates. The curing process was performed in an autoclave with a vacuum bag pressure of −850 mbar and an external pressure of 6 bar. The temperature was firstly set at 50 °C for 30 min, and subsequently maintained at 100 °C for 4 h, with heating ramps of 1 °C/min. The first heating step at 50 °C was adopted to favor the impregnation of the nanofiber mats within the epoxy resin of the laminate, by decreasing the viscosity of the epoxy matrix without triggering the cross-linking. The second step allowed the full reticulation of the resin (T_g = 120 °C), according to the supplier, without overcoming the melting temperature of the Nylon and P(VDF-TrFE) nanofibers (270 °C and 145 °C respectively). The resulting curing thickness for the self-sensing and the reference was 2.12 ± 0.06 mm and 2.09 ± 0.04 mm, respectively.

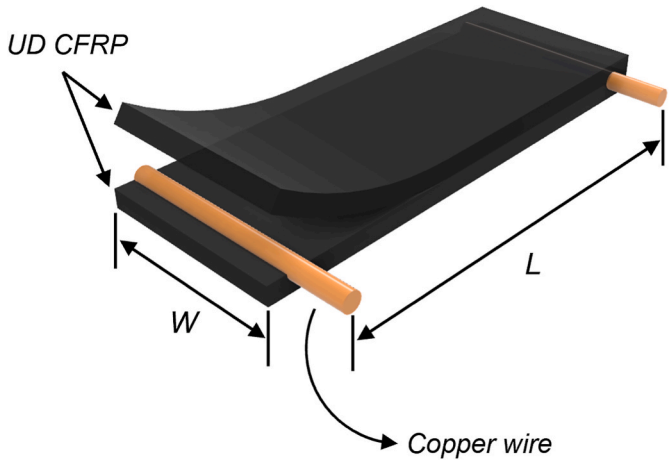

Fig. 1. Schematic representation of the connections between the copper wires and the carbon fibers.

2.1.4. Poling

In P(VDF-TrFE), the β phase of the crystalline lattice is the one responsible for the piezoelectric behavior. The electrospinning process favors the formation of the β phase due to the stretching of the nanofibers during the deposition on the drum collector [48]. However, to induce a macroscale piezoelectric behavior, a poling process is required to align the ferroelectric domains in the same direction. P(VDF-TrFE) thin films are usually polarized by applying an external electric field, which uniformly distributes along the material thickness [49,50]. When piezoelectric elements – such as nanofibers or sub-micrometric particles – are dispersed in the epoxy resin of a composite material, the electric field distributes unevenly between the two materials according to their electrical properties and volumetric fractions.

In this work, during the curing cycle, the P(VDF-TrFE) nanofibrous membranes are embedded between the plies of the composite laminate, and the interconnected air channels are filled by the epoxy resin, thus generating a bi-component system. As the poling electric field is applied on the self-sensing laminate, it acts differently on both phases, as studied in detail in previous works [18,51]. The polarization process was carried out by applying an electric field of 10 kV/mm for 10 min at 100 °C, close to the Curie temperature (T_c = 103 °C) of P(VDF-TrFE) to facilitate the dipole movement. The electric field was applied by connecting the high voltage generator (Keithley, Model 248 High Voltage supply) to the copper wires interleaved between the two pairs of CFRP plies adjacent to the piezoelectric layer, serving as signal electrodes. Since the copper wire is electrically connected to the CFRP plies (see Section 2.1.2), this arrangement ensured the transmission of the high voltage to the carbon fibers, exploiting them for the polarization process. After the poling process, the signal electrodes were connected to the ground for 24 h to remove any residual electrostatic charge, which could affect the acquisition of the piezoelectric signal.

2.2. Electromechanical characterizations

To assess the sensing performances of the laminate, a prior investigation of the electrical properties of the nanofibrous interlayers was carried out. Resistance and capacitance measurements between adjacent electrodes were performed using an RLC meter (GW-Instek 6002) set in parallel configuration. In particular, the effectiveness of the Nylon nanofibers insulating interlayer was verified by connecting the RLC meter between the shield and the signal electrodes, both in the top and bottom sides of the laminate. Similarly, the same measurements were repeated across the two signal electrodes, which sandwich the P(VDF-TrFE) nanofibrous layer at the midplane.

The aforementioned interlayer measurements were used to define the sensitivity S, the capacitance C, and the effective piezoelectric strain coefficient d_{33}^{eff} of the self-sensing laminate. The sensitivity S was calculated as the ratio between the peak-to-peak output voltage and the peak-to-peak input compressive load (mV/kN), as expressed in Equation (1).

$$S = (V_{max} - V_{max}) / (F_{max} - F_{min}) \quad (1)$$

The sensitivity of each self-sensing laminate was calculated with both the shield electrodes connected to the ground (S_{shield}) and left floated ($S_{no\ shield}$). According to the method described in Ref. [44], the effective piezoelectric strain coefficient d_{33}^{eff} can be calculated according to Equation (2).

$$d_{33}^{eff} = S_{shield} * C_{shield} = S_{no\ shield} * C_{no\ shield} \quad (2)$$

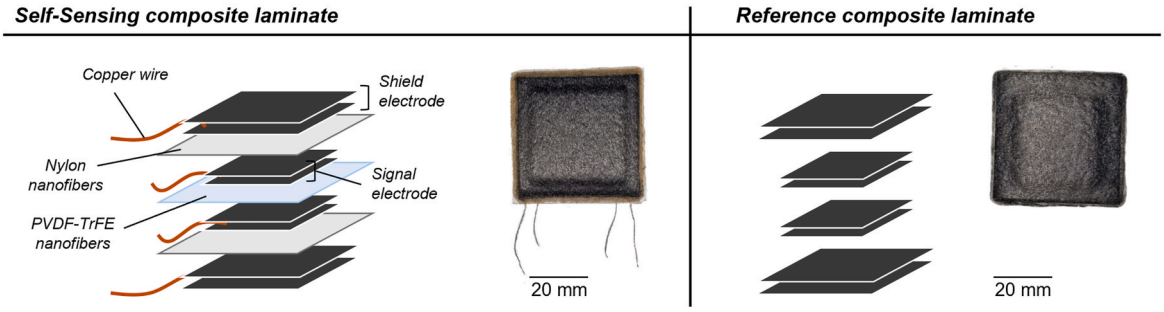

Fig. 2. Stacking sequence of the self-sensing and reference laminates.

where C_{shield} and $C_{no\ shield}$ are the capacitances of the composite laminates measured across the signal electrodes for the shielded and the no shielded configurations, respectively. It is worth pointing out that d_{33}^{eff} is a property of the material (P(VDF-TrFE) nanofibers embedded in the epoxy resin), and it can be calculated both in the shield and not shielded configurations.

Experimentally, a compressive sinusoidal load oscillating between 0.6 and 1.1 kN at 20 Hz was applied to the laminates, by using an Instron 8033 hydraulic testing machine equipped with a 25 kN load cell. A plastic cylindrical indenter with a diameter of 10 mm was mounted on the machine. To facilitate the electrical connections with the acquisition circuit, the copper wires were soldered with electric cables (red and black signal cables, green and yellow shield cables), as shown in Fig. 3. The cables of the signal electrodes were connected to an INA118. Specifically, the thin copper wires of the CFRP-based electrodes were soldered to external cables (colored cables of Fig. 3) for an easier connection to the acquisition circuit during testing. A resistance $R_{shunt} = 1\ G\Omega$ was connected in parallel to the input of the amplifier, and both the load cell and piezoelectric signals were simultaneously acquired at a frequency of 2 kHz. A detailed discussion of the acquisition circuit and the equivalent lumped electric circuit has been presented in previous works [18,44].

It is worth pointing out that the use of a preload was necessary to properly calculate also the $S_{no\ shield}$, as the absence of shield electrodes would lead to triboelectric noise in case of friction or brushing between the indenter and the sensing laminate.

2.3. Low velocity impact test

Low-velocity impact tests (LVI) were performed both on the self-sensing and reference laminates to investigate the effect of the nanofibers interleaving on the impact strength and the piezoelectrical behavior during an impact event.

The tests were conducted following the ASTM D7136 standard [52], using a drop-weight machine with a 1.3 kg impactor mass equipped with a PCB 208C05 load cell and 12.7 mm hemispherical steel tip. To adapt to the small dimensions of the laminates, the specimens were leaned on a support plate with a cylindric hole with a diameter of 20 mm. A laser device was used to monitor the pre- and post-impact velocity of the impactor, as shown in Fig. 4. Both the laser device and load cell signals were simultaneously acquired at 100 kHz. Both laminate types were impacted at three different energy levels equal to 1.5, 3, and 6 J with three repetitions. After polishing, micrograph analyses of the cross-section on the impact point were performed to evaluate the damage type (i.e., cracks or delamination) both for the self-sensing and reference laminates. Beyond the mechanical evaluation, the piezoelectric signals were recorded during the LVI with the same signal conditioning electric circuit of Section 2.2. In particular, preliminary

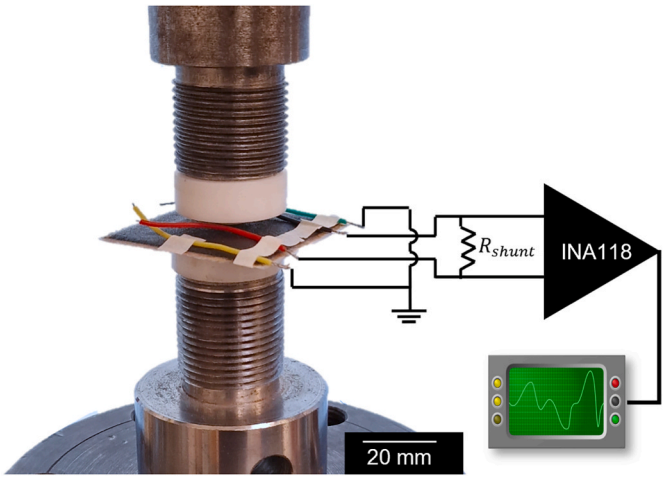

Fig. 3. Cyclic force indentation setup and piezoelectric signal acquisition.

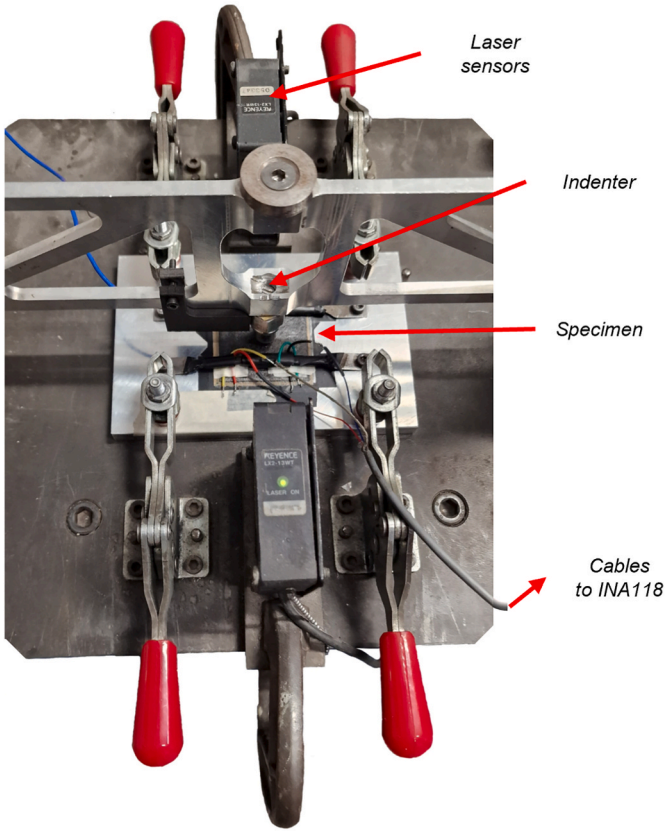

Fig. 4. LVI test setup.

non-destructive LVIs with an impact force equal to 0.3 kN were performed before and after the destructive LVI tests to evaluate any alterations in the sensitivity of the laminates induced by the destructive impacts for each energy level.

In the end, as a further quantification of electromechanical damages caused by the destructive LVI, interlayer electrical resistance and capacitance measurements were repeated after the test with the same procedure described in Section 2.2.

3. Results & discussion

3.1. CFRP electrodes optimization

The electrical resistance of CFRP-based electrodes was tested as outlined in Section 2.1.2. The resistance values, measured between copper wires placed at the edge of the samples, were plotted against the length (L), as shown in Fig. 5a–. b, and Fig. 5c. The slope of the regression lines (dashed lines) were 0.06 Ω/cm, 0.32 Ω/cm, and 164.80 Ω/cm for the [0°,0°], [0°,90°], and [90°,90°] configurations, respectively, indicating the resistance per unit length of the CFRP-based electrodes. The process of embedding copper wires between CFRP plies involves the presence of a contact resistance R_C, which is estimated as the y-intercept of the linear regression [39]. In the [0°,90°] configuration, the contact resistance is minimal, about 0.02 Ω, and can be considered negligible. However, in the [90°,90°] configuration, the resistance is so high that the contact resistance is not measurable. In Fig. 5d, the electrical conductivities of the three types of CFRP-based electrodes are shown, assuming a homogenous and continuous material structure. The [0°,0°] configuration has the highest conductivity, but it also contains a noticeable eye-shaped resin pocket, which can affect the mechanical properties of the hosting laminate, as revealed by the scanning electron microscope (SEM) image. The [90°,90°] configuration has much higher resistance because the transverse conduction relies on contact between neighboring fibers [39,53]. Given these factors, the [0°,90°] configuration is the best compromise, offering a conductivity similar to the [0°,0°] configuration (see bar graph of Fig. 5d) but with better integration within the 90° oriented carbon fiber layer. Moreover, having fibers oriented in both principal directions is expected to result in similar conductivity. Therefore, the [0°,90°] configuration represents an effective method to fabricate in-situ electrodes, which can be exploited both for the polarization process and the piezoelectric signal collection [44].

3.2. Laminate morphology

The staking sequence of the autonomous self-sensing composite

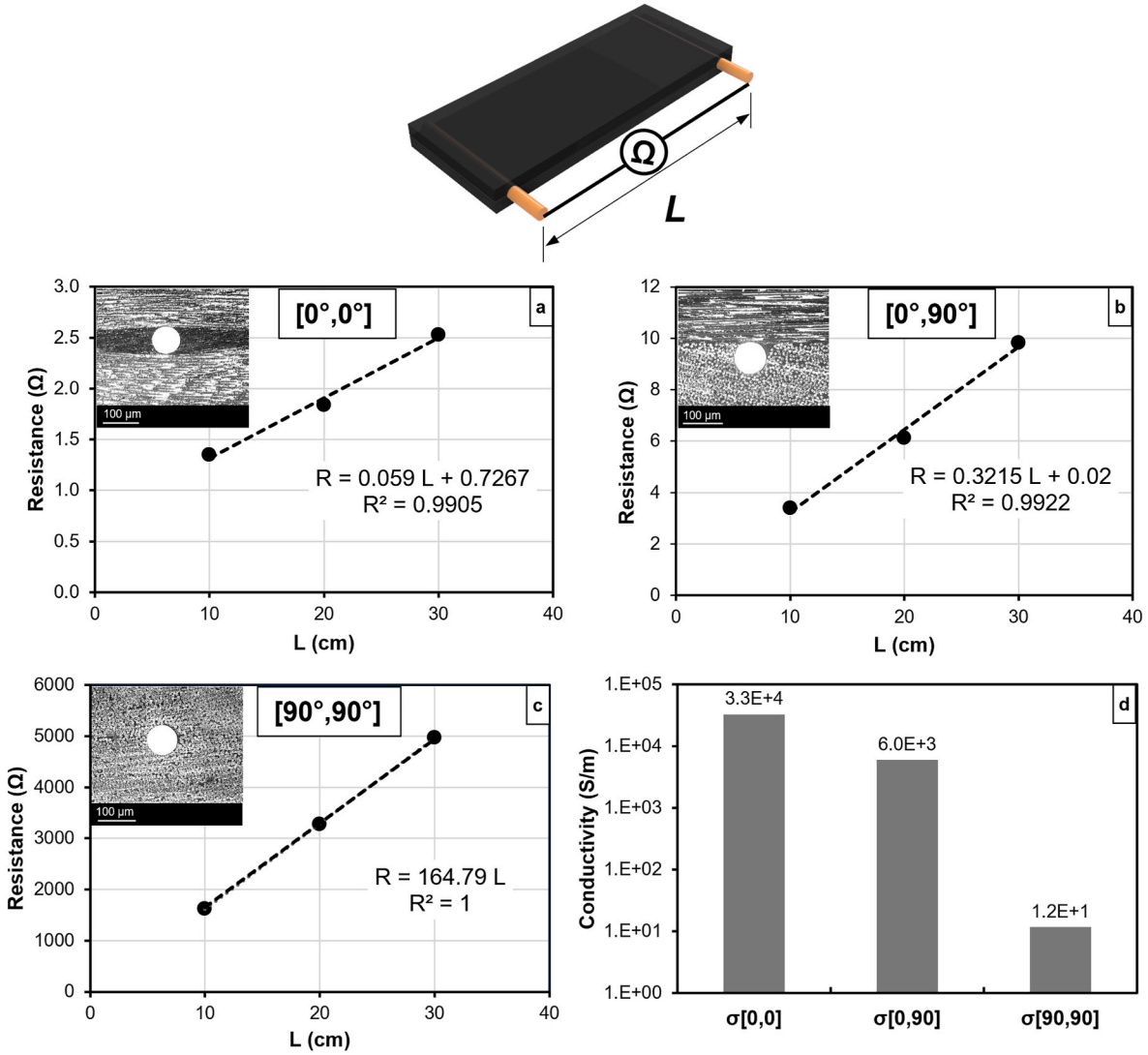

Fig. 5. Electrical resistance vs length of CFRP-based electrodes for the a) [0°,0°], b) [90°,0°] and c) [90°,90°] configurations; d) electrical conductivity of the three types of electrodes.

material proposed in this study is schematically represented in Fig. 6, where the SEM magnifications provide a visual description of the main characteristics of the laminate.

The SEM images Fig. 6a and b show the nanofibers morphology of the piezoelectric material as spun (P(VDF-TrFE)), and the insulating material (Nylon), respectively. In both membranes, the nanofibers appear randomly oriented and bead-free, with an average diameter equal to 513.8 ± 82.9 nm for PVDF-TrFE and 141.7 ± 22.2 nm for Nylon nanofibers, calculated via SIMpoly algorithm [54].

As described in Section 2.1.3, the P(VDF-TrFE) nanofibrous mat was interleaved in the composite laminate midplane, serving as an electric charge generator for mechanical sensing (Fig. 6d). The adjacent CFRP plies serve as electrodes to collect the piezoelectric signal. The latter are sandwiched between two Nylon nanofiber membranes to electrically insulate them from the outer shield CFRP electrodes (Fig. 6e). The entire stacking sequence is clearly observable in the SEM cross-section view of Fig. 6c. In the SEM magnification of Fig. 6d and e the good impregnation of the nanofibers within the epoxy resin of the laminate is visible for P(VDF-TrFE) and Nylon nanofibers, respectively. The piezoelectric P(VDF-TrFE) nanofibers are visible as bright dots in the SEM images due to the higher electrical conductivity compared to the surrounding epoxy resin. On the contrary, to make the Nylon nanofibers visible, the sample was soaked for 15 min in a chloroform bath to dissolve and remove them. In this way, the Nylon nanofibers appear as holes in the SEM magnification of Fig. 6e. In both cases, no voids are visible in the cross-sections, meaning a good impregnation of the nanofiber membranes by the epoxy resin and a perfect integration with the composite laminate.

Finally, Fig. 6f reports an SEM magnification of the embedding of the copper wires into the CFRP electrodes. According to the procedure described in Section 2.1.2, the copper wire is sandwiched between a UD CFRP oriented at 90° and one oriented at 0°. During the curing cycle, the carbon fibers which are transversally disposed to the copper cable (i.e., the UD CFRP at 0°) force the wire to immerse into the 90°-oriented ply, with carbon fibers parallel to it. This phenomenon prevents the formation of any eye-shaped resin pockets.

3.3. Composite piezoelectric properties

As observed in Section 2.1.2 and in previous works [39,53], the electrical resistivity through the thickness (which can be considered equal to the transversal direction) is at least two orders of magnitude greater than resistivity in the longitudinal direction. The interleaving of a nanofibrous mat between two prepreg plies generates a resin-rich meatus integrated with nanofibers (see Fig. 6d and e), serving as a dielectric barrier. Consequently, these sandwich-like structures can be considered as the set of plane capacitors, with the CFRP plies working as electrodes. Consistently with the nano-modified laminate structure, three interlayer electric measurements of resistance and capacitance were performed before the LVI, as detailed in Section 2.2. Fig. 7 graphs the resistance and capacitance average values for each interlayer: Nylon-based dielectric layers (labeled (1) and (3)) and the PVDF-TrFE-based piezoelectric one (labeled (2)). It can be observed that the capacitance is slightly higher for the piezoelectric layer compared to the insulating ones (1.32 nF vs 1.12 nF). This can be attributed to the higher dielectric constant of the P(VDF-TrFE) compared to the Nylon one. Instead, the resistance values are statistically comparable (average value equal to 5.37 MΩ).

From a self-sensing performance perspective, the laminate was characterized in terms of sensitivity, linearity and d_{33}^{eff}. The output voltage signal and the applied load vs time are graphed in Fig. 8a and b, both for the shielded (S_{shield}) and no-shielded ($S_{no\ shield}$) configuration (see Section 2.2). The mean sensitivity of all specimens is 335 ± 22.0 mV/kN for the unshielded configuration, while the mean sensitivity for the shielded one reaches 233 ± 10.6 mV/kN, corresponding to an average decrement of 30 %. As expected, this reduction is due to the higher equivalent capacity of the whole self-sensing laminate in the shielded configuration. However, as demonstrated in Ref. [37], in real-environment applications the shield electrodes are necessary to remove triboelectric noise and electromagnetic interference.

To evaluate the sensor linearity, the output voltage values are plotted in Fig. 8c as a function of a cycle of compressive force between 0.6 and 1.1 kN, where a null voltage is noticeable when the force is equal to the

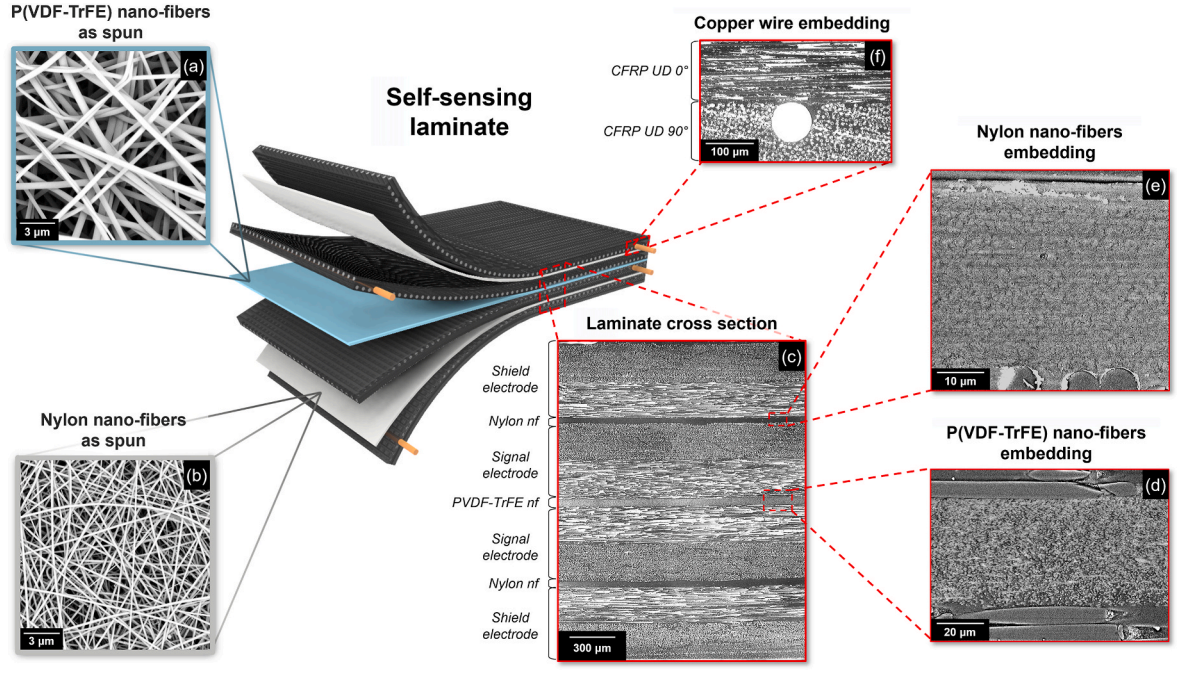

Fig. 6. Schematic representation of the autonomous self-sensing composite laminate and SEM magnification of a) P(VDF-TrFE) and b) Nylon nanofibers as spun; c) cross-section of the laminate; d) P(VDF-TrFE) and e) Nylon nanofibers embedded within the laminate plies; f) cross-section of the CFRP-based electrode, with copper wire embedded.

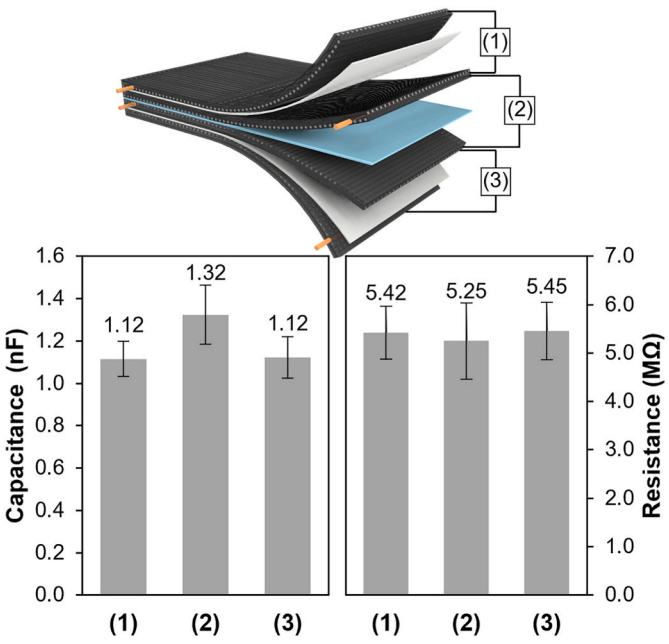

Fig. 7. Intralayer resistance and capacitance measurements.

preload (−0.85 kN). This behavior is due to the working principle of the piezoelectric sensor, which works as a charge generator. Being the electric charges dissipated during time, the information about the initial static preload is lost, and only the cyclic dynamic load is detected. This phenomenon has been accurately investigated in Ref. [51]. Moreover, since the piezoelectric working environment is highly dynamic, potential changes in thermal conditions would not affect the piezoelectric performance, as these are relatively long-time events. The only temperature limitation regards the Curie temperature of the piezoelectric material (T_c = 103 °C), beyond which the ferroelectric dipoles undergo random reorientation, resulting in a loss of piezoelectric properties.

In Fig. 8d the spatial response homogeneity of the self-sensing laminate on its whole surface is plotted (sensitivity of 345 ± 10.4 mV/kN).

By multiplying the sensitivity values with corresponding capacitances (see Equation (2)), it is possible to evaluate the effective piezoelectric strain coefficient of the piezoelectric nanostructured interlayer (d_{33}^{eff}) [18]. As expected, the d_{33}^{eff} values measured in the shielded and unshielded configurations are comparable and equal to −0.4 ± 0.04 pC/N, thus demonstrating that the cause of the sensitivity variation is the different capacitance of the two configurations [44].

3.4. Impact performances

3.4.1. Impact resistance and micrograph analyses

The impact resistance of the autonomous self-sensing composite laminates was evaluated according to the procedure described in Section 2.3, both for the self-sensing and reference laminates. In Fig. 9 the force vs displacement graphs of the self-sensing and reference composite materials are reported for the three impact energy levels. As it can be observed, the stiffnesses of the two types of laminate are comparable, as the initial slopes of the curves overlap. For all the impact energies, a first force curve drop is visible in the range between 1.5 and 2 kN, and it can be associated with fiber breakages or delamination that lead to a stiffness reduction [5]. By comparing the behavior of the two different types of laminate, it is observable that the first drop occurs before in the reference laminates than the self-sensing ones, for all the energy impact levels. Moreover, a higher maximum displacement is observed for the reference laminate, pointing out a stiffness reduction due to the higher damage. This behavior is also confirmed by the absorbed–impact energy ratio reported in the bar graph of Fig. 10. Generally, the highest values of

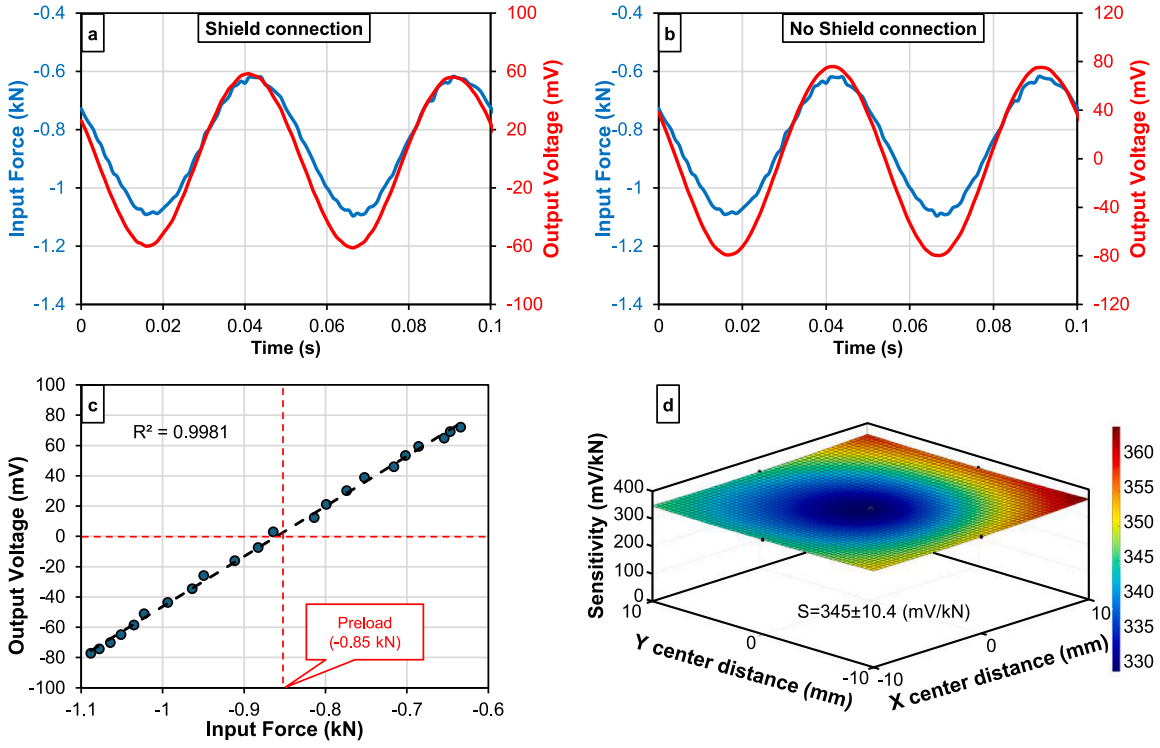

Fig. 8. Piezoelectric voltage during compressive cyclic loads in the case of a) shielded and b) no-shielded configuration; c) output piezoelectric voltage vs compressive force d) sensitivity value of the laminate across the self-sensing laminate surface.

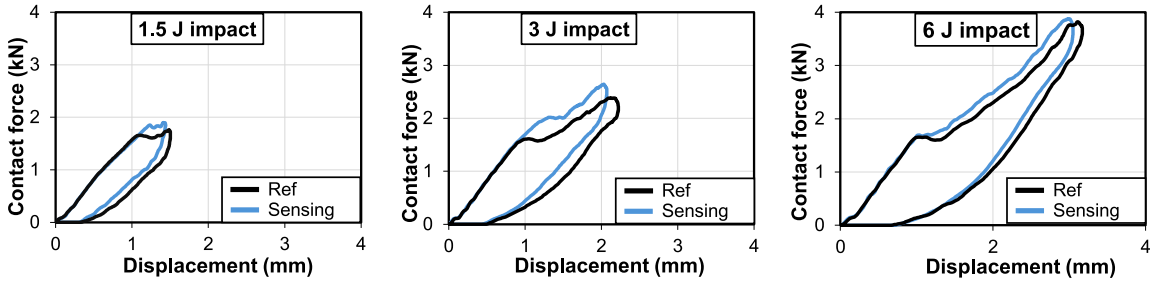

Fig. 9. Contact force vs displacement graphs of the self-sensing and reference laminates, at three energy impact levels.

absorbed energy are measured for reference laminates, whereas the absorbed energy decreases when nanofibers are interleaved between the plies of the composite material, especially for lower impact energies.

Since the absorbed impact energy is mainly related to high-energy absorption mechanisms such as viscous damping and fiber breakage [5], micrograph analyses were performed to investigate low-energy absorbing events, such as delamination and matrix cracking. Fig. 11 depicts only half of the cross-sections of the laminates, as the damage is symmetrical to the impact point. The left and right sides of the panel illustrate the reference and self-sensing laminates, respectively, while the rows refer to the different impact energy levels. For each laminate, the fiber breakage, delamination, and matrix crack lengths are measured and reported in the bar graphs in Fig. 12.

At an impact energy of 1.5 J, the reference laminate exhibits small 45° oriented cracks with a reverse pine tree pattern (red arrows), suggesting a predominant Hertzian contact stress [5]. Matrix cracks propagate then as delamination at the interface between the CFRP UD layer oriented at 0° and the one oriented at 90°. Instead, delamination (blue arrows) is negligible for the self-sensing laminate, where the nanofibers are discernible in the cross-section as brighter interlayers. Indeed, the presence of the Nylon nanofibrous mat prevents delamination between the CFRP signal electrode and the shield one, considerably reducing the delamination length. On the contrary, intralayer transversal matrix cracks are comparable because they cannot be hindered by the nanofibers that are positioned in the interlayers.

A similar trend is observed in the case of the 3 J impact test. The cracks propagate between the laminate plies of the reference laminate, leading to extended delamination with a total length of 16.8 mm, which is three times higher than the delamination length of the corresponding self-sensing laminate (5.3 mm). On the other hand, a higher number of cracks oriented at 45° and the fiber breakage (green arrows) is visible in the self-sensing laminate, as also remarked in the bar graphs of Fig. 12.

Similarly, in the case of a 6 J impact, the presence of nanofibrous layers mitigates the delamination propagation between adjacent CFRP plies, but a higher number of transversal cracks and fiber breakage can be observed.

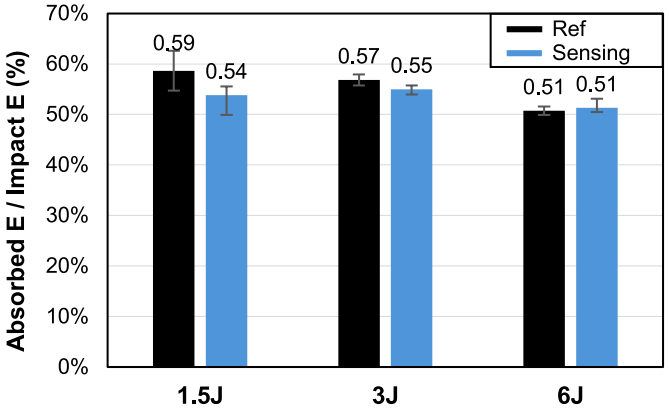

Fig. 10. Absorbed energy values of each laminate during the LVI tests.

Generally, the embedding of a tough thermoplastic nanofibrous mats (both Nylon and PVDF-TrFE) within the fragile thermoset epoxy resin generates a thin meatus with a higher degree of fracture toughness [31]. When the crack front bumps into this nano-toughened interlayer, a large amount of energy is required to extend the crack as delamination. At this point, the easiest way to dissipate the energy is fiber breakage or matrix cracks, as quantitatively confirmed in the bar graphs of Fig. 12.

In conclusion, the main effect of the nanofibers interleaving is the remarkable reduction of delamination for all the impact energy levels, in a range between 70 % (for the 3 J impact) and 90 % (for the 6 J impact). Consequently, the impact energy dissipates as matrix cracks and fiber breakage, whose values consistently increase, especially for higher energy levels.

3.4.2. *Real-time impact SHM*

For a comprehensive understanding of the operating range of the self-sensing laminate, non-destructive and destructive mechanical impacts were performed on the laminates. This approach aimed to differentiate between the regions subjected to impact loads that exhibit a linear sensing response and those where the sensing capability is compromised.

A preliminary non-destructive test was performed on the self-sensing laminate by applying a mechanical impact with a contact force lower than 0.4 kN. In Fig. 13, it is observable that the piezoelectric output voltage curve accurately follows the contact force one measured by the load cell, thus detecting the highly dynamic event (~0.3 ms).

In the graph of Fig. 14 the sensitivity S can be calculated as the slope of the linear regression of the piezoelectric signal plotted as a function of the contact force. The S value is equal to 226 mV/kN with, and it is consistent with the sensitivity values measured during the compressive cyclic loads in the shielded configuration (see Section 3.3). In this region, the mechanical impact does not induce damage to the laminate, and the correlation between the output voltage and the applied load is linear ($R^2 = 0.994$).

Subsequent analyses were performed to determine the piezoelectric behavior during destructive impacts. The graphs of Fig. 15 report the contact force and the piezoelectric output signal during the destructive LVI at different impact energy levels. As observable for the 1.5 J impact (Fig. 15a), the load cell signal trend is not reproduced by the piezoelectric signal, due to mechanical damages which occur during the impact. The output voltage raises up to 8 V (saturation level of the instrumentation amplifier INA118) in correspondence with the region where the first breakage mechanisms occur, likely due to mechanical damages induced to carbon fibers, which move during impact and alter the proper sensing mechanism. A similar trend is observable in Fig. 15b and c for higher impact energy levels (i.e., 3 J and 6 J), where the destructive impacts a more severe damage amount. Indeed, such high-energy impacts are responsible for the breakage of carbon fibers, which penetrate the P(VDF-TrFE) membrane during the impact, thus inducing a short circuit between the two signal electrodes. This assumption finds a correspondence in the voltage drop of the LVI graphs

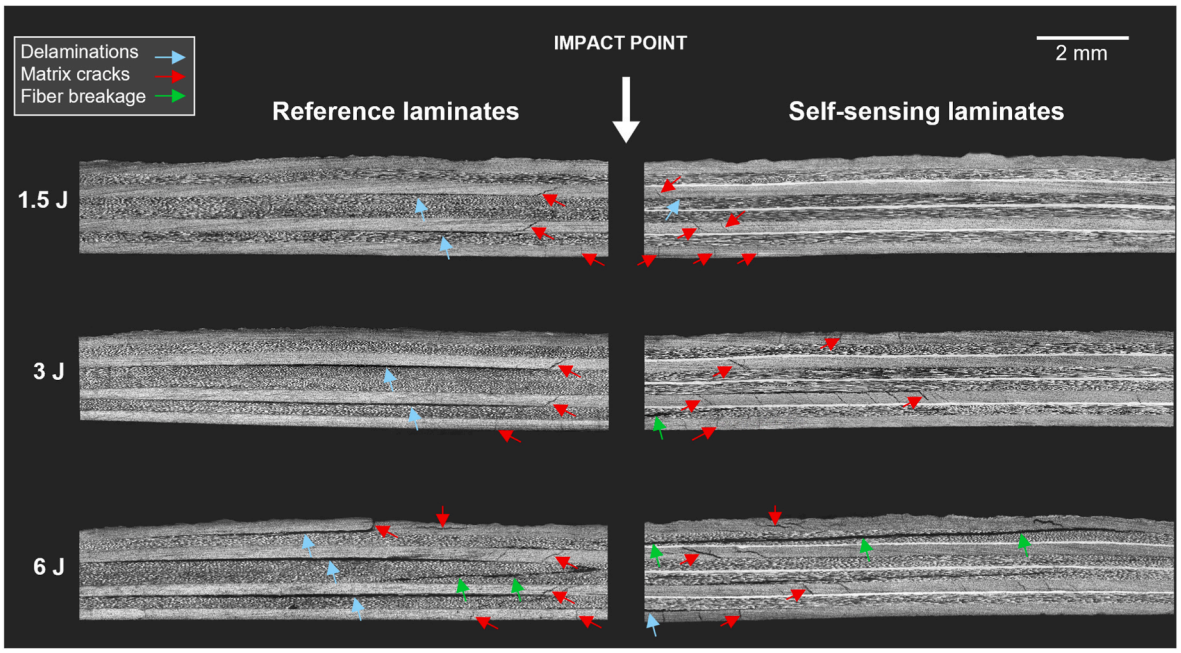

Fig. 11. Micrographs analyses of the cross-section of both the reference and self-sensing laminates, after the LVI tests.

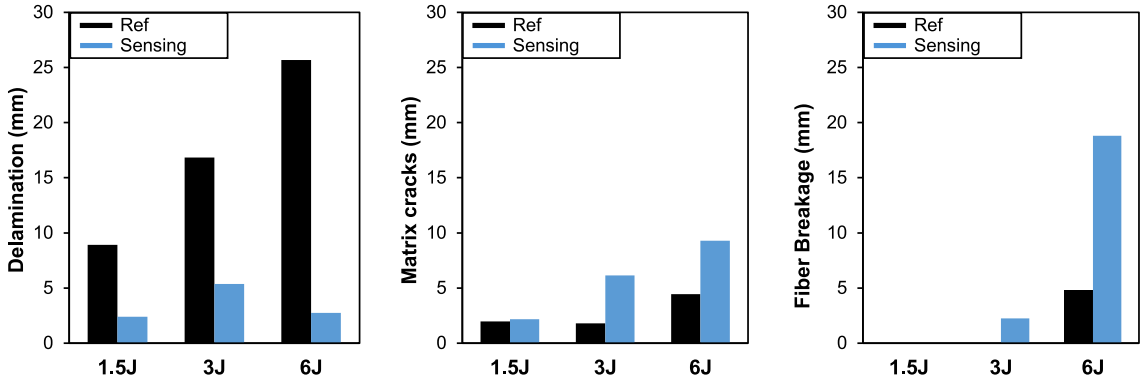

Fig. 12. Delamination, matrix cracks and fiber breakage length for each laminate, for each energy level of LVI test.

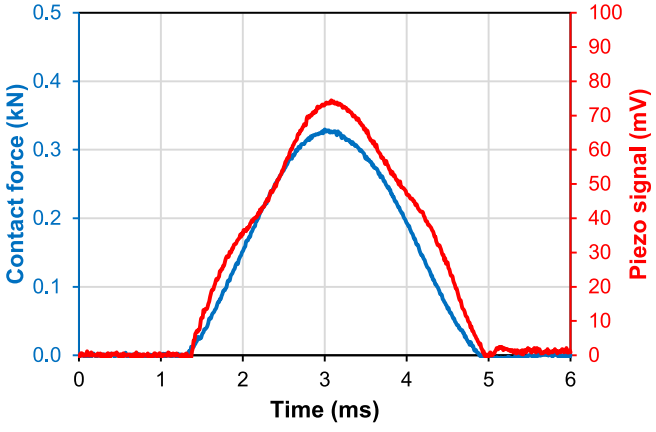

Fig. 13. Non-destructive impact test.

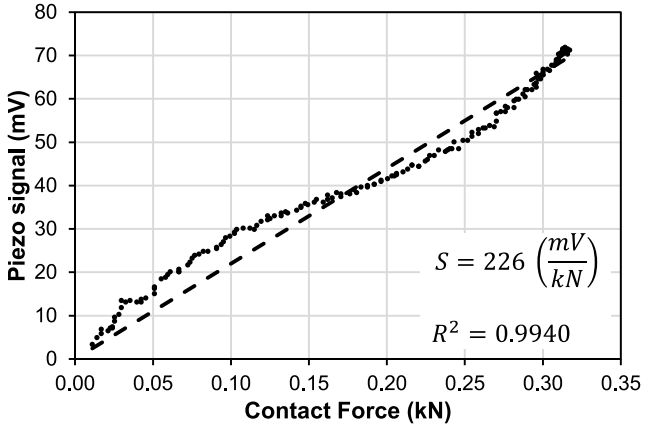

Fig. 14. Piezo-signal vs contact force graphs in the case of a non-destructive impact test.

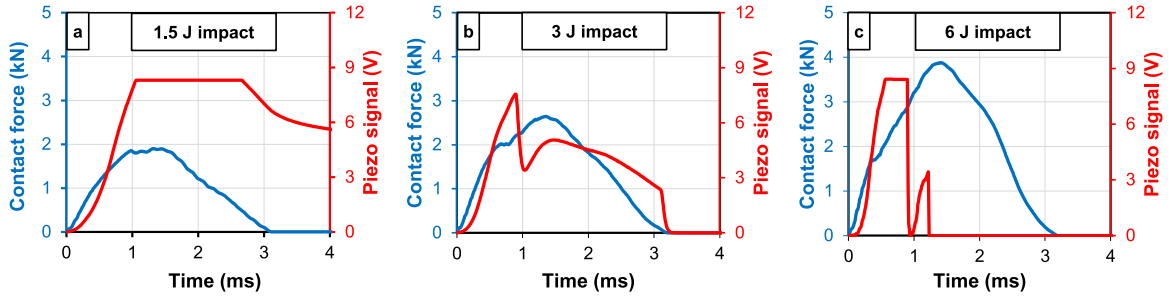

Fig. 15. Contact force vs piezo-signal graphs of the LVI tests of the self-sensing laminates for impact energy equal to a) 1.5 J, b) 3 J and c) 6 J.

of 3 J and 6 J (Fig. 15b and c, respectively), which occurs in the force range between 2 and 3 kN, as the result of carbon fibers' contact.

This behavior indicates the presence of a threshold in the amplitude of contact force that initiates mechanical damage and permanently compromises the linear response of the self-sensing laminate, hence the sensor itself. Indeed, as shown in the piezoelectric voltage vs contact force graph of Fig. 16, the signal proportionality is compromised after a contact force equal to 0.6 kN. Beyond this value, there is a noticeable deviation between the dashed line and the curves corresponding to the LVI tests, indicating the occurrence of mechanical damage that significantly alters the linear proportionality. In a SMH perspective, this sudden nonproportional increase in voltage can be exploited as a real-time trigger of a notable impact event that may have compromised the structural integrity of the component (see Fig. 16).

Moreover, the high sensitivity allows for scale-up of the self-sensing laminate dimensions to fabricate components for real applications. Indeed, since the sensitivity is inversely related to the capacitance and the capacitance is proportional to the laminate area (see Equation (2)), the latter is constrained by the signal-to-noise ratio. Given a noise level of 0.1 mV in the measuring system and a resolution target of 0.1 kN, the maximum permissible area for the self-sensing laminate can be estimated as 0.75 x 0.75 m^2. This value makes it possible to produce autonomous self-sensing laminates with dimensions feasible for the composite materials industry, taking this technology beyond the confines of research laboratories.

3.4.3. Post-impact SHM

Further measurements were conducted to evaluate the integrity of the interlayer insulation, following the method described in Section 2.2. In the bar graph of Fig. 17, the capacitances and resistances after impact for different energy levels are normalized to the respective values before impact. It can be observed that the values do not reveal any remarkable changes except for those between the electrodes in the case of the 3J and 6J impacts. In particular, a slight drop in the capacitance ratio can be observed for the 3 and 6 J of about ~ - 20 % in the nF range. Concerning the resistance, the values drop of about four orders of magnitude (from MΩ to 100 Ω), highlighting a severe interlayer breakage caused by delamination and fiber breakage that short circuit the adjacent layers working as electrodes.

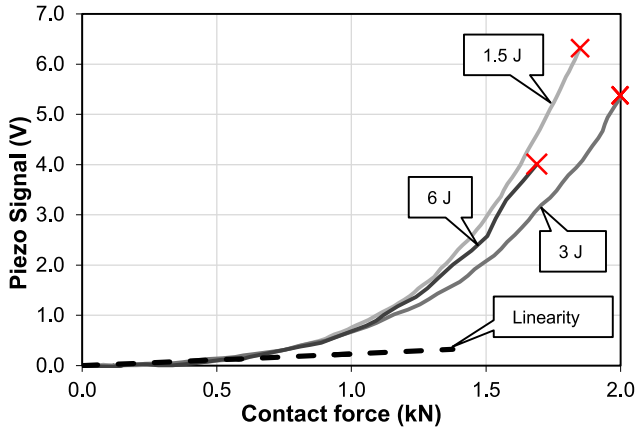

Fig. 16. Piezo-signal vs contact force during the first portion of the destructive impact tests.

Therefore, as described in the previous Section 3.4.2, the impact event can be detected by a piezoelectric signal when it exceeds the proportionality value defined by the sensitivity (SHM by real-time impact load detection). Then, to assess the damage after impact, electrical resistance measurements between interlayers can be performed (SHM post-event damage evaluation).

4. Conclusions

This study presents a novel approach to SHM in composite materials by integrating self-sensing capabilities into a CFRP laminate without compromising its mechanical performance. The self-sensing structure includes P(VDF-TrFE) nanofibers interleaved at the midplane, with adjacent CFRP plies serving as electrodes to capture piezoelectric signals. To mitigate noise, additional CFRP plies (shield electrodes) were electrically insulated from the signal electrodes using Nylon 6,6 nanofibers. After poling, the laminate demonstrated high sensitivity (233 ± 10.6 mV/kN) and effective piezoelectric coefficient ($d_{33}^{eff} = -0.44 \pm 0.04$ pC/N) in response to mechanical impacts.

Mechanically, low-velocity impact (LVI) tests revealed enhanced impact resistance in the self-sensing laminate compared to its non-sensing counterpart. The nanofiber interleaving increased interlaminar fracture toughness and reduced delamination, as confirmed by micrograph analysis. The laminate is capable of detecting real-time impact on its whole surface and evaluating its magnitude for real-time SHM application. Furthermore, it can monitor interlaminar damage after impact by detecting changes in the electrical resistance of the CFRP interlayers for post-event SHM or NDE applications.

In conclusion, this work introduces, for the first time, a laminate that combines self-sensing functionality with improved impact resistance. These advancements position the piezoelectric laminate as a promising material for aerospace and automotive applications, offering a new avenue for self-sensing composites.

CRediT authorship contribution statement

Francesco Mongioì: Writing – original draft, Methodology, Investigation, Formal analysis, Data curation, Conceptualization. **Giacomo Selleri:** Writing – original draft, Methodology, Investigation, Formal analysis, Data curation, Conceptualization. **Emanuele Maccaferri:** Writing – review & editing, Methodology, Investigation. **Davide Fabiani:** Writing – review & editing, Supervision, Conceptualization. **Andrea Zucchelli:** Writing – review & editing, Writing – original draft, Supervision, Conceptualization. **Tommaso Maria Brugo:** Writing –

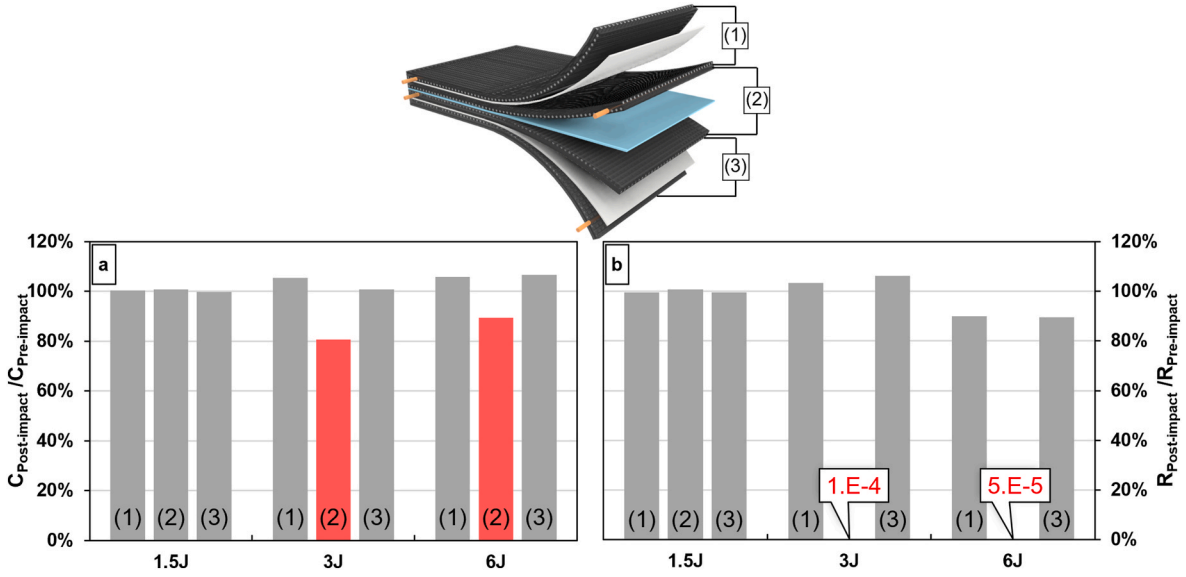

Fig. 17. Interlayer electrical measurements of a) capacitance and b) resistance, expressed as their ratio after and before the LVI at 1.5, 3 and 6 J.

original draft, Supervision, Methodology, Investigation, Formal analysis, Conceptualization.

Declaration of competing interest

The authors declare that they have no known competing financial interests or personal relationships that could have appeared to influence the work reported in this paper.

Acknowledgements

This research was funded by PRIN 2022 PNRR SELF-RE-PREG: Self-Sensing Interleaving for Recycled Prepreg (CUP: J53D23015920001), by European Union NextGenerationEU - National Sustainable Mobility Center (CN00000023) Spoke 11 - Innovative Materials & Lightweighting, by the Project Ecosyster - Ecosystem for Sustainable Transition in Emilia-Romagna (CUP J33C22001240001), and by CYPHER Project (CUP: E37G22000470007) and PRIN 2022 Project 3DSHYMCO (CUP: J53D23002470006). The authors would like to thank Solvay and Alessio Marrani for providing the polymers and BA student Dario Röper for contributing in the development of the autonomous sensing laminate.

Data availability

Data will be made available on request.

References

[1] Giurgiutiu V. Introduction. In: Structural health monitoring of aerospace composites. Elsevier; 2016. p. 1–23. https://doi.org/10.1016/b978-0-12-409605-9.00001-5.
[2] Kausar A. Aeronautical composites and materials. In: Polymeric nanocomposites with carbonaceous nanofillers for aerospace applications. Elsevier; 2023. p. 1–21. https://doi.org/10.1016/B978-0-323-99657-0.00016-8.
[3] Zhang J, Lin G, Vaidya U, Wang H. Past, present and future prospective of global carbon fibre composite developments and applications. Compos B Eng Feb. 2023; 250:110463. https://doi.org/10.1016/j.compositesb.2022.110463.
[4] Wang CH. Progressive multi-scale modelling of composite laminates. In: Multi-scale modelling of composite material systems: the art of predictive damage modelling. Elsevier; 2005. p. 259–77. https://doi.org/10.1533/9781845690847.259.
[5] Abrate Serge. Impact on composite structures. Cambridge University Press; 2005.
[6] Giurgiutiu V. Damage and failure of aerospace composites. In: Structural health monitoring of aerospace composites. Elsevier; 2016. p. 125–75. https://doi.org/10.1016/b978-0-12-409605-9.00005-2.
[7] Zeng X, Zhao B, Liu X, Yu Y, Guo J, Qing X. Lamb wave-based damage assessment for CFRP composite structures using a CHMM-based damage localization algorithm and a damage quantitative expression. Mech Syst Signal Process 2023;184(April 2022):109750. https://doi.org/10.1016/j.ymssp.2022.109750.
[8] Oh HT, Won JI, Woo SC, Kim TW. Determination of impact damage in cfrp via pvdf signal analysis with support vector machine. Materials 2020;13(22):1–23. https://doi.org/10.3390/ma13225207.
[9] He Q, Li X, Zhang H, Briscoe J. Nano-engineered carbon fibre-based piezoelectric smart composites for energy harvesting and self-powered sensing. Adv Funct Mater 2023;33(20). https://doi.org/10.1002/adfm.202213918.
[10] Cai J, Qiu L, Yuan S, Shi L, Liu P, Liang D. Structural health monitoring for composite materials. In: Composites and their applications. InTech; 2012. https://doi.org/10.5772/48215. ch. 3.
[11] Masmoudi S, El Mahi A, Turki S. Use of piezoelectric as acoustic emission sensor for in situ monitoring of composite structures. Compos B Eng 2015;80:307–20. https://doi.org/10.1016/j.compositesb.2015.06.003.
[12] Gabardi M, et al. Embedding fiber bragg grating sensors in carbon composite structures for accurate strain measurement. IEEE Sensor J 2023;23(15):16882–92. https://doi.org/10.1109/JSEN.2023.3285408.
[13] Oromiehie E, Prusty BG, Compston P, Rajan G. In situ process monitoring for automated fibre placement using fibre Bragg grating sensors. Struct Health Monit 2016;15(6):706–14. https://doi.org/10.1177/1475921716658616.
[14] Oromiehie E, Prusty BG, Compston P, Rajan G. Characterization of process-induced defects in automated fiber placement manufacturing of composites using fiber Bragg grating sensors. Struct Health Monit 2018;17(1):108–17. https://doi.org/10.1177/1475921716685935.
[15] Takeda N, Okabe Y, Kuwahara J, Kojima S, Ogisu T. Development of smart composite structures with small-diameter fiber Bragg grating sensors for damage detection: quantitative evaluation of delamination length in CFRP laminates using Lamb wave sensing. Compos Sci Technol Dec. 2005;65(15–16):2575–87. https://doi.org/10.1016/J.COMPSCITECH.2005.07.014.
[16] Wang HP, Chen C, Ni YQ, Jayawickrema M, Epaarachchi J. Computer-aided feature recognition of CFRP plates based on real-time strain fields reflected from FBG measured signals. Compos B Eng Aug. 2023;263:110866. https://doi.org/10.1016/J.COMPOSITESB.2023.110866.
[17] Wang HP, Ni YQ, Dai JG, Yuan MD. Interfacial debonding detection of strengthened steel structures by using smart CFRP-FBG composites. Smart Mater Struct 2019;28(11). https://doi.org/10.1088/1361-665X/ab3add.
[18] Gino ME, et al. On the design of a piezoelectric self-sensing smart composite laminate. Mater Des 2022;219:110783. https://doi.org/10.1016/j.matdes.2022.110783.
[19] Rocha H, Semprimoschnig C, Nunes JP. Sensors for process and structural health monitoring of aerospace composites: a review. Eng Struct Jun. 2021;237:112231. https://doi.org/10.1016/J.ENGSTRUCT.2021.112231.
[20] Ramakrishnan M, Rajan G, Semenova Y, Farrell G. Overview of fiber optic sensor technologies for strain/temperature sensing applications in composite materials. Sensors (Switzerland) 2016;16(1). https://doi.org/10.3390/s16010099.
[21] Shivakumar K, Bhargava A. Failure mechanics of a composite laminate embedded with a fiber optic sensor. J Compos Mater 2005;39(9):777–98. https://doi.org/10.1177/0021998305048156.
[22] Konka HP, Wahab MA, Lian K. The effects of embedded piezoelectric fiber composite sensors on the structural integrity of glass-fiber-epoxy composite laminate. Smart Mater Struct 2012;21(1). https://doi.org/10.1088/0964-1726/21/1/015016.

[23] Yu Y, Shi Y, Kurita H, Jia Y, Wang Z, Narita F. Carbon fiber-reinforced piezoelectric nanocomposites: design, fabrication and evaluation for damage detection and energy harvesting. Compos Part A Appl Sci Manuf 2023;172(January):107587. https://doi.org/10.1016/j.compositesa.2023.107587.
[24] Hwang MY, Kang LH. Characteristics and fabrication of piezoelectric GFRP using smart resin prepreg for detecting impact signals. Compos Sci Technol 2018;167 (July):224–33. https://doi.org/10.1016/j.compscitech.2018.08.002.
[25] De Rosa IM, Sarasini F. Use of PVDF as acoustic emission sensor for in situ monitoring of mechanical behaviour of glass/epoxy laminates. Polym Test Sep. 2010;29(6):749–58. https://doi.org/10.1016/J.POLYMERTESTING.2010.04.006.
[26] Zhang F, et al. Embedded Pt-PVDF sensor without compromising mechanical properties of GFRP for on-line sensing. Thin-Walled Struct 2023;187(March): 110702. https://doi.org/10.1016/j.tws.2023.110702.
[27] Bae JH, Lee SW, Chang SH. Characterization of low-velocity impact-induced damages in carbon/epoxy composite laminates using a poly(vinylidene fluoride–trifluoroethylene) film sensor. Compos B Eng 2018;135(August 2017): 189–200. https://doi.org/10.1016/j.compositesb.2017.10.008.
[28] Brugo T, Palazzetti R. The effect of thickness of Nylon 6,6 nanofibrous mat on Modes I–II fracture mechanics of UD and woven composite laminates. Compos Struct Oct. 2016;154:172–8. https://doi.org/10.1016/J.COMPSTRUCT.2016.07.034.
[29] Zarei H, Brugo T, Belcari J, Bisadi H, Minak G, Zucchelli A. Low velocity impact damage assessment of GLARE fiber-metal laminates interleaved by Nylon 6,6 nanofiber mats. Compos Struct May 2017;167:123–31. https://doi.org/10.1016/J.COMPSTRUCT.2017.01.079.
[30] Palazzetti R, Zucchelli A. Electrospun nanofibers as reinforcement for composite laminates materials – a review. Compos Struct Dec. 2017;182:711–27. https://doi.org/10.1016/J.COMPSTRUCT.2017.09.021.
[31] Daelemans L, Van Der Heijden S, De Baere I, Rahier H, Van Paepegem W, De Clerck K. Damage-resistant composites using electrospun nanofibers: a multiscale analysis of the toughening mechanisms. ACS Appl Mater Interfaces 2016;8(18): 11806–18. https://doi.org/10.1021/acsami.6b02247.
[32] Daelemans L, Verschatse O, Heirman L, Van Paepegem W, De Clerck K. Toughening mechanisms responsible for excellent crack resistance in thermoplastic nanofiber reinforced epoxies through in-situ optical and scanning electron microscopy. Compos Sci Technol Jan. 2021;201:108504. https://doi.org/10.1016/J.COMPSCITECH.2020.108504.
[33] Saghafi H, et al. The thickness effect of rubbery nanofibrous mat on modes I–II fracture mechanism of composite laminates. Thin-Walled Struct 2024;196 (December 2023):111556. https://doi.org/10.1016/j.tws.2024.111556.
[34] Jakubczak P, Bieniaś J, Surowska B. Impact resistance and damage of fiber metal laminates. In: Hybrid polymer composite materials. Elsevier; 2017. p. 279–309. https://doi.org/10.1016/B978-0-08-100787-7.00012-3.
[35] Mathivanan P, Balakrishnan M, Krishnan H. Metal thickness, fiber volume fraction effect on the tensile properties, debonding of hybrid laminates. J Reinforc Plast Compos 2010;29(14):2128–40. https://doi.org/10.1177/0731684409345616.
[36] Niazi M, Sadr MH. Numerical shear buckling investigation of GLAREs with initial delamination. Adv Mater Sci Eng 2022;2022. https://doi.org/10.1155/2022/9059917.
[37] Brugo TM, et al. Self-sensing hybrid composite laminate by piezoelectric nanofibers interleaving. Compos B Eng 2021;212(February):108673. https://doi.org/10.1016/j.compositesb.2021.108673.
[38] Safarova V, Gregr J. Electrical conductivity measurement of fibers and yarns. 7th international conference-TEXSCI. 2010. p. 2–9.
[39] Abry JC, Bochard S, Chateauminois A, Salvia M, Giraud G. In situ detection of damage in CFRP laminates by electrical resistance measurements. Compos Sci Technol 1999;59(6 SPEC. SEC):925–35. https://doi.org/10.1016/S0266-3538(98)00132-8.
[40] Iwasaki A, Todoroki A. Statistical evaluation of modified electrical resistance change method for delamination monitoring of CFRP plate. Struct Health Monit 2005;4(2):119–36. https://doi.org/10.1177/1475921705049757.
[41] Yu Y, Luo C, Chiba H, Shi Y, Narita F. Energy harvesting and wireless communication by carbon fiber-reinforced polymer-enhanced piezoelectric nanocomposites. Nano Energy 2023;113(May):108588. https://doi.org/10.1016/j.nanoen.2023.108588.
[42] Yu Y, Luo C, Suto T, Uetsuji Y, Narita F. Fabrication, evaluation, and multiscale simulation of piezoelectric composites reinforced using unidirectional carbon fibers for flexible motion sensors. Small 2024;20(24):1–14. https://doi.org/10.1002/smll.202307689.
[43] Wang Z, Kurita H, Nagaoka H, Narita F. Potassium sodium niobate lead-free piezoelectric nanocomposite generators based on carbon-fiber-reinforced polymer electrodes for energy-harvesting structures. Compos Sci Technol 2020;199(July): 108331. https://doi.org/10.1016/j.compscitech.2020.108331.
[44] Mongioì F, Selleri G, Maria Brugo T, Maccaferri E, Fabiani D, Zucchelli A. Multifunctional composite material based on piezoelectric nanofibers and Cu-CFRP electrodes for sensing applications. Compos Struct 2024;337(March):118076. https://doi.org/10.1016/j.compstruct.2024.118076.
[45] Todoroki A, Tanaka M, Shimamura Y. Measurement of orthotropic electric conductance of CFRP laminates and analysis of the effect on delamination monitoring with an electric resistance change method. Compos Sci Technol 2002; 62(5):619–28. https://doi.org/10.1016/S0266-3538(02)00019-2.
[46] Palazzetti R, Yan X, Zucchelli A. Influence of geometrical features of electrospun nylon 6,6 interleave on the CFRP laminates mechanical properties. Polym Compos Jan. 2014;35(1):137–50. https://doi.org/10.1002/pc.22643.
[47] Palazzetti R, et al. Influence of electrospun Nylon 6,6 nanofibrous mats on the interlaminar properties of Gr–epoxy composite laminates. Compos Struct Jan. 2012;94(2):571–9. https://doi.org/10.1016/j.compstruct.2011.08.019.
[48] Calavalle F, Zaccaria M, Selleri G, Cramer T, Fabiani D, Fraboni B. Piezoelectric and electrostatic properties of electrospun PVDF-TrFE nanofibers and their role in electromechanical transduction in nanogenerators and strain sensors. Macromol Mater Eng 2020;305(7):1–8. https://doi.org/10.1002/mame.202000162.
[49] Chan HLW, et al. Polarization of thick polyvinylidene fluoride/trifluoroethylene copolymer films. J Appl Phys 1996;80(7):3982–91. https://doi.org/10.1063/1.363356.
[50] Eberle G, Bihler E, Eisenmenger W. Polarization dynamics of VDF-TrFE copolymers. IEEE Trans Electr Insul 1991;26(1):69–77. https://doi.org/10.1109/14.68230.
[51] Selleri G, et al. Self-sensing composite material based on piezoelectric nanofibers. Mater Des 2022;219:110787. https://doi.org/10.1016/j.matdes.2022.110787.
[52] ASTM D7136. Standard test method for measuring the damage resistance of a fiber-reinforced polymer matrix composite to a drop-weight impact event. 2012. https://doi.org/10.1520/D7136.
[53] Todoroki A, Tanaka M, Shimamura Y. Electrical resistance change method for monitoring delaminations of CFRP laminates: effect of spacing between electrodes. Compos Sci Technol 2005;65(1):37–46. https://doi.org/10.1016/j.compscitech.2004.05.018.
[54] Murphy R, Turcott A, Banuelos L, Dowey E, Goodwin B, Cardinal KOH. SIMPoly: a matlab-based image analysis tool to measure electrospun polymer scaffold fiber diameter. Tissue Eng C Methods 2020;26(12):628–36. https://doi.org/10.1089/ten.tec.2020.0304.